Chiral nematic droplets with tangential anchoring and negative dielectric anisotropy in an electric field

J. Bajc,* J. Bezić, and S. Žumer
Physics Department, University of Ljubljana, Jadranska 19, 61000 Ljubljana, Slovenia
(Received 9 August 1994)

Model structures for the droplets of chiral nematic (cholesteric) liquid crystals with negative dielectric anisotropy exposed to the external electric field are developed. For tangential anchoring with no preferred direction a field induced transformation from structures with spherical chiral nematic surfaces via intermediate structures with ellipsoidal surfaces to planar structures is described. Two different spherical structures corresponding to defect lines with strength 1 and 2 are taken as the initial states. The number, type, and shape of χ disclination lines which occur in such systems are explained in detail.

PACS number(s): 64.70.Md, 61.30.Gd, 61.30.Jf

I. INTRODUCTION

Recently, several polarizing microscope studies of the electric field effect on the chiral nematic (N^*) droplets with negative dielectric anisotropy have been reported [1,2]. The structure of the N^* phase is determined by two "fields"—the nematic director field $\vec{n}(\vec{r})$, which shows the average direction of the long axis of the molecules, and the twist field $\vec{q}(\vec{r})$, which points in the direction of the axis about which the director $\vec{n}$ is rotating [3]. Even if the molecules of the N^* phase do not possess the mirror symmetry along their long axis, the directions $\vec{n}$ and $-\vec{n}$ are equivalent. This is because they have the same amount of molecules in a particular direction and in the opposite direction. The wave vector $\vec{q}$, on the other hand, is a regular vector and its length depends on the rotation rate of the direction $\vec{n}$. The change of the sign of $\vec{q}$ results in the change of the sense of rotation of the director $\vec{n}$. In an unconstrained chiral nematic phase the nematic director field exhibits a uniform twist with the director everywhere tangential to mutually parallel planes. The corresponding field of twist axes (twist field) $\vec{q}$ with $q=2\pi/(\text{pitch})$ is thus homogeneous. It is convenient to describe the N^* phase with the so-called N^* (or cholesteric) surfaces, which are defined as the surfaces that are everywhere perpendicular to the vector $\vec{q}$. For homogeneous twist field these surfaces are planes, while they will be quite complicated when the twist field is more general. The presence of defects or boundaries strongly deforms the director field, so the N^* surfaces are ill defined in their vicinity. If these anomalies are neglected, one refers to nondegenerate N^* surfaces. This approximation is frequently quite suitable [4]. When an external electric or magnetic field is applied an undeformed structure of N^* planes is expected only in systems with negative dielectric or magnetic anisotropy if the applied field is parallel to the twist axis. The confinement to droplets breaks the symmetry of the N^* phase and thus results in more general structures with N^* planes deformed into N^* surfaces [5]. The disclination lines in the director field (χ lines) and in the twist field (λ lines) appear [6]. If there is no external field and droplets are spherical, the N^* surfaces are also spherical [6–8] [see Figs. 1(a) and 1(b)]. The systems with negative dielectric anisotropy described in Refs. [1,2] exhibit a field induced transformation from a structure with spherical N^* surfaces characteristic of low external fields, to a structure with planar surfaces [9–11] characteristic of high fields [see Fig. 1(c)]. The observations of intermediate textures made with a polarizing microscope indicate that in such droplets the radial spherical structure [7] has the radial χ line oriented perpendicular to the electric field. As the electric field increases, the radial χ line rotates in a plane perpendicular to the electric field. Simultaneously, a circle grows from the center of the texture. When examined by crossed polarizers parallel to the applied electric field, uniform color of the texture inside the circle is observed [2,6]. This indicates relatively planar N^* surfaces. The fingerprint pattern outside the circle indicates tilted and curved N^* surfaces [2]. In a special case, when the cholesteric pitch is bigger than $\frac{1}{5}$ of the droplet radius ($2\pi/q > R/5$), the distance between lines in the fingerprint pattern decreases with increasing electric field and the radial χ line keeps a fixed orientation in a plane perpendicular to the electric field [2,6].

In both cases, in the plane parallel to the electric field the lines in the fingerprint pattern are ellipses [6], which encouraged the development of the model structures presented in this paper [12].

In some cases, when the electric field (2.0 V/μm) was abruptly switched off, metastable states appeared [6]. The authors report that many circles occurring in parallel planes perpendicular to the electric field were observed. The circles gradually shrink and combine into a single circle. Before the resulting circle completely vanishes, a structural transition, which starts in one hemisphere, occurs "in the entire droplet" [6].

In this paper, model structures will be generated using the approximation of nondegenerate N^* surfaces and strong planar anchoring on the droplet surface [7,10].

*Corresponding author.

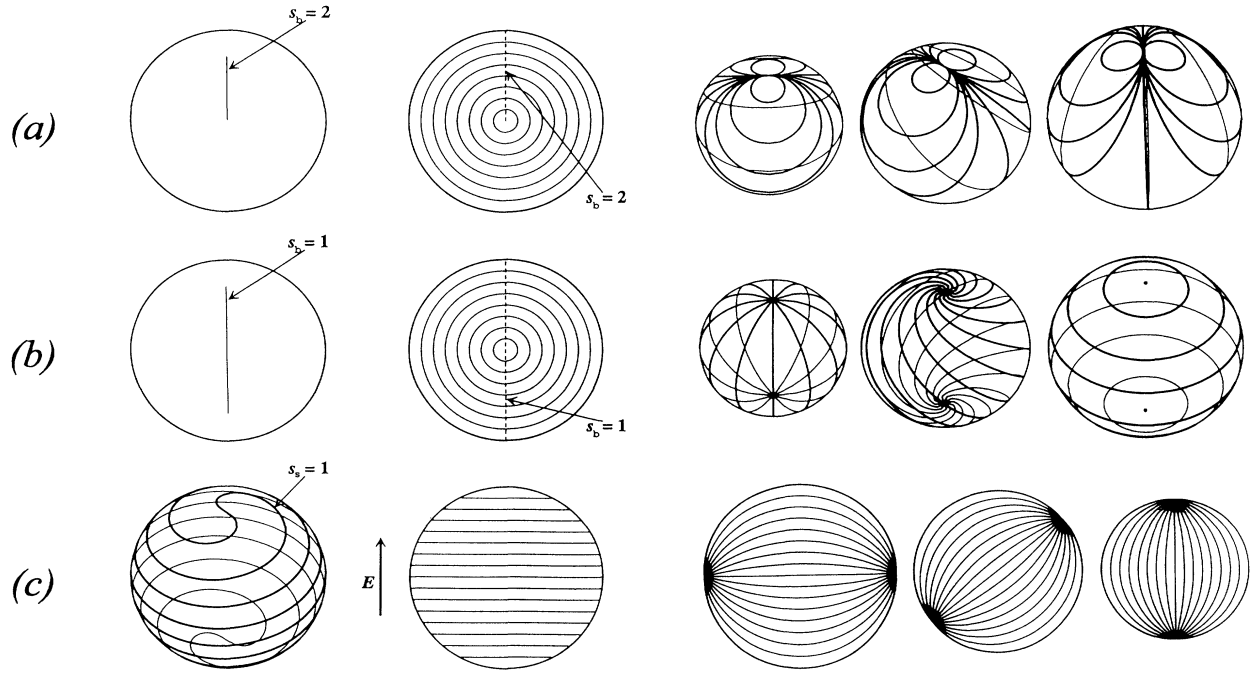

FIG. 1. (a) Radial spherical structure (RSS), (b) diametrical spherical structure (DSS), and (c) planar bipolar structure (PBS). All the left-hand sketches show a 3D view of χ disclination lines with their bulk strengths s. These lines are bulk lines for spherical structures (a), (b) and surface lines for planar bipolar structure (c). The middle sketches show cross sections of the droplets. The N^* surfaces are planes on (c) and concentric spheres on (a), (b). The middle sketches also show bulk χ lines (a), (b). On the right-hand sketches the director fields on several N^* spheres (a), (b) and N^* planes (c) are shown. Radial configuration of helical axes in spherical structures (a), (b) results in the relative rotation of director configuration on successive N^* spheres. On the other hand, the helical axes are parallel to the z axis in planar bipolar structure (c) and this results in the relative rotation of director configuration on successive N^* circles along the z axis.

Strong anchoring means that the molecules (as well as the director) are fixed at the surface—in the case of strong planar anchoring their long axes are parallel to the surface. It will further be supposed that droplets are large compared to the cholesteric pitch. The first step is to find appropriate N^* surfaces. In Sec. II we introduce rotational ellipsoids as N^* surfaces which allow a continuous transformation between concentric spheres in spherical structures and planes in planar structures. The director $\vec{n}$ is everywhere tangential to such surfaces; thus, a director field on an N^* surface is equivalent to a director field of a two-dimensional (2D) nematic surface. Consequently, all symmetry allowed defects of a 2D nematic phase are found on an N^* surface [10]. Connecting 2D nematic defects on sequences of N^* surfaces χ lines are modeled. The approximation of nondegenerate N^* surfaces is improved by introducing escaped cores of finite radii around χ lines of integer strength [10]. In Sec. III the model structures are described in detail. In Sec. IV the approximate free energy is written [9]. In Sec. V results are summarized and briefly compared to experimental observations.

II. SEARCH FOR POSSIBLE STRUCTURES

It has been shown theoretically [10,7] and observed experimentally [1,2,6,9] that stable structures in the absence of external field are the ones with spherical N^* surfaces. Simple solutions for the director field in droplets with spherical structures were found in our previous paper [10],

$$\vec{n}=\cos\Omega\vec{e}_\vartheta+\sin\Omega\vec{e}_\varphi\ ,\quad \Omega=(s-1)\varphi+qr+\Omega_0\ , \tag{1}$$

where s is the strength of the χ defect line along the $+z$ axis. As we have shown, according to the topological theory another defect line of strength $2-s$ along the $-z$ axis must appear [10,13,14]. Because of the relation between the two defect lines, the parameter s is enough to characterize the spherical structures. The three most stable spherical structures are radial ($s=2$), double radial ($s=\frac{3}{2}$), and diametrical ($s=1$) structure [10]. Here we will consider only the radial [Fig. 1(a)] and the diametrical [Fig. 1(b)] spherical structures as the possible initial structures. The former, first proposed by Frank and Pryce (pages 41–42 of Ref. [8]), has been observed experimentally and the latter, according to our theoretical results, has the lowest free energy [10]. Free energy, as well as topological description of chiral nematic phase in spherical droplets, will be discussed in detail in the following sections. It is also known that negative dielectric (or magnetic) anisotropy in a high electric (or magnetic) field favors structures with planar N^* surfaces. Experiments are carried out mainly in the electric field because the dielectric anisotropy can be much larger than the magnetic anisotropy. As the experiments showed con-

tinuous transformation from spherical to planar structures, the natural choice for a simple model of N^* surfaces appearing at intermediate fields is an oblate rotational ellipsoid. In cylindrical coordinates (ρ,ϕ,z) with the z axis parallel to the electric field, such surfaces can be described with

$$\frac{\rho^2}{(r+\delta)^2}+\frac{z^2}{r^2}=1 , \tag{2}$$

where r is the length of the short axis of the ellipsoid oriented along the z axis and $r+\delta$ is the length of the long axis of the ellipsoid. The variation of the parameter δ can thus describe a continuous spherical-to-planar structure transformation from $\delta=0$, where the N^* surfaces are concentric spheres, to $\delta\rightarrow\infty$, where N^* surfaces are planes normal to the z axis.

In droplets of radius R the rotational ellipsoids with $r+\delta<R$ and $\delta>0$ lie completely inside the droplet [see Fig. 2(a)]. All defects of the 2D nematic director field confined to such closed surfaces are internal (bulk) defects. Their strengths s_i must satisfy the relation [10,15]

$$\sum s_i=2 . \tag{3}$$

From ellipsoidal surfaces with $R-\delta<r\leq R$, the surface of the droplet, that is, the sphere of radius R, cuts two caps [Fig. 2(a)]. On the boundary (circumference) of the upper and lower cap the director field must be tangential to satisfy the strong planar anchoring condition imposed by the droplet surface. Such nonclosed 2D nematic surfaces have both internal and boundary type defects in the director field. Here boundary refers to circumference and internal to the interior of the 2D nematic surface. Therefore, the sum of the corresponding defect strengths on each cap must, according to the definition of the strength of the boundary defects [16], satisfy

$$\sum s_i^{\text{bulk}}+\frac{1}{2}\sum s_j^{\text{boundary}}=1 . \tag{4}$$

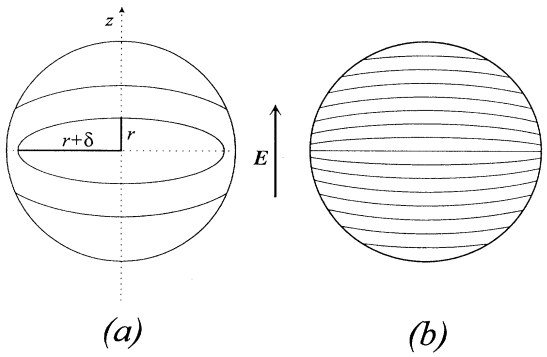

FIG. 2. (a) Examples of two different types of N^* surfaces. For $r+\delta<R$ the N^* surface is closed. For $r+\delta>R$ the N^* surface is cut into two caps of oblate rotational ellipsoids. (b) The N^* surfaces when $\epsilon=\delta/R$ equal 1. The N^* surfaces are here very similar to the ones on the middle Fig. 1(c). On both figures the z axis coincides with the direction of the electric field. The N^* surfaces are cylindrically symmetrical—the axis of symmetry is the z axis.

In the special case $r=0$ where the rotational ellipsoid degenerates into a circle, the circumference of this circle is singular in the field of helical axes. As is known from homotopy theory [13,14], the disclination lines in N^* phases are singular in either the director or the twist field or in both fields. Here the director field, which is tangential to the circumference of the circle, is not singular, but the helical axes, which are everywhere normal to the N^* surface at the circumference, rotate for π around the edge. Thus, the circumference of the $r=0$ circle is a λ disclination line of the strength $\frac{1}{2}$ [3].

The arguments applied for nematic circles in Ref. [16] can here be applied to caps of rotational ellipsoids. The initial state in this contribution is one of the spherical structures. In this structure the cholesteric twist is satisfied in the radial direction according to expression (1). When the electric field is applied along the z axis, initially spherical N^* surfaces expand in the direction perpendicular to the z axis. As a result, the N^* surfaces are deformed to the rotational ellipsoids. It is important to keep in mind that the spheres are deformed in the xy direction only, the deformation being described by the parameter δ introduced in Eq. (2) [see Fig. 2(a)]. The director configuration near the z axis, does not change much because of this deformation. The cholesteric twist is therefore satisfied along the z axis as qz. In ellipsoidal structures the parameter that characterizes a particular N^* surface is r, introduced by Eq. (2). As the short axis of the oblate rotational ellipsoidal N^* surfaces coincides with the z axis, expressions qz and qr are equivalent near the z axis. This indicates that the simplest approximation for the cholesteric twist in ellipsoidal structures is qr, where r is the short axis of the ellipsoid. In the limit $\delta=0$, qr is precisely the radial cholesteric twist and in the limit $\delta\rightarrow\infty$ the N^* surfaces inside the droplet are planes with cholesteric twist qr, which is in this case equivalent to qz. At intermediate δ the field of helical axes changes from radial to uniform configuration via the so-called cholesteric axial field $\vec{q}(\vec{r})$ [6]. The radial arrangement is transformed into the uniform configuration via a hyperboliclike arrangement of helical axes. This approximation is thus consistent with the spherical-to-planar transition. As a crude estimate one could say that the structure on the closed ellipsoidal N^* surfaces $(r+\delta<R)$ is the same as the structure on the corresponding spherical N^* surfaces. The structures on the rotational ellipsoidal caps $(r+\delta>R)$ are, however, similar to the structures on the nematic circles described in [16]. The particular cap is characterized by the short axis of the ellipsoid r and the cholesteric twist remains qr.

The shapes of the spirals on the surface of the spherical droplets with ellipsoidal structures can be obtained by following the expressions in Ref. [16] and substituting all products qz with products qr. Obtaining the shape of spirals, it must be kept in mind that the range of r on the droplet surface is

$$R-\delta<r<R \tag{5}$$

and that the lower bound $(R-\delta)$ decreases as the parameter δ increases.

III. ELLIPSOIDAL STRUCTURES

Equipped with the model for the N^* surfaces at intermediate electric field, we can describe various ellipsoidal structures in more detail. In this section the ellipsoidal structures will be described topologically and in the next section the free energies and the stability of particular intermediate structures will be estimated. We need only the following facts about the relation between the electric field and the ellipsoidal structures.

(1) The ellipsoidal N^* surfaces are oriented in electric field with their short axes parallel to the applied electric field (z axis of the coordinate system).

(2) The bulk χ defect lines lie either parallel or perpendicular to the applied electric field. This will be proved later when free energy is considered.

(3) Each ellipsoidal structure is characterized by the parameter δ or, equivalently, by the dimensionless parameter $\epsilon \equiv \delta/R$. As the electric field is increased to intermediate values the parameter δ is increased to values larger than zero [see Eq. (2)].

There are three qualitatively different regimes, $\epsilon=0$, $0<\epsilon<1$, and $1<\epsilon$. When $\epsilon=0$ the structures are spherical. In this case the N^* surfaces are closed spheres. In the second regime the ellipsoidal structures show up. This regime will be of primary interest from now on. In the third regime the structures are still ellipsoidal in the sense that N^* surfaces are parts of oblate rotational ellipsoids, but all N^* surfaces are nonclosed and quite flat [see Fig. 2(b)]. So in this regime the structures are almost planar; one can describe them as slightly deformed planar structures.

The droplets with ellipsoidal structures ($0<\epsilon<1$) can be divided into three regions with different defect configurations. In the first one the N^* surfaces are closed ellipsoids ($r<R-\delta$). The bulk defects that originate from the spherical structures are sufficient in this region [Eq. (3)] and no additional defect lines are needed. In the second region the N^* surfaces are caps of rotational ellipsoids so Eq. (4) is valid. There might be some bulk defects that originate from the spherical structures in this region, but since Eq. (3) is not valid, some additional defect lines might be needed. This region is characterized by $R-\delta<r<r(\delta)$, where $r(\delta)$ is calculated numerically from

$$\frac{R^2-\delta^2}{r^2}+\frac{\delta^2}{(r+\delta)^2}=1 \Longrightarrow r=r(\delta)\ . \tag{6}$$

In the third region [$r(\delta)<r<R$] there are no bulk defects and the two surface $s=1$ χ lines suffice. There could be other defect configurations in this region satisfying Eq. (4), but none of them would lead to the planar bipolar structure (PBS), which has the minimal free energy [10] among the planar structures in a droplet. The χ defect lines in the last two regions are formed by combining point defects on each N^* cap, which is cut off from the rotational ellipsoid by the sphere of radius R. The bulk defect line is a combination of interior defects on the N^* surfaces, while the surface defect line is a combination of boundary defects on the N^* surfaces. When constructing various ellipsoidal structures that lead from spherical to planar structures, one must take into account topological and energetical constraints. The structures that will appear in nature must strictly satisfy topological constraints. This has been described in Sec. II and is used hereafter. Energetical constraints are not taken so strictly, because we would like to cover also metastable structures, which are often observed although their free energy is not a global minimum. Ellipsoidal structures that are presented below are all topologically possible, although some of them have not yet been observed, probably because they are metastable.

The term "spiral" is frequently used for the surface defect lines. By using this terminology we want to stress the helical shape of the surface defect lines. Let us first describe common features of these defect lines. For very small nonzero ϵ the surface defect lines are not helical, because the region $R-\delta<r<R$ is much smaller than the pitch. When ϵ is increased the surface defect lines become more and more helical. In spite of this general behavior, the surface defect lines near the equatorial plane persist in nonhelical shape [see, for example, Figs. 3(a) and 4(b)]. This happens because the N^* surfaces at the edge of the equatorial circle are tangential to the droplet surface for each $\epsilon<1$ [Fig. 2(a)]. As a consequence a small increase of r results in a large increase of the z coordinate of the circumference of the N^* cap. The surface line defects are formed by combining boundary defects on N^* caps and a small change in r results in a small rotation of the director field and thus in a small rotation of the surface defect line. It follows that the surface χ defect line is perpendicular to the equatorial circle. This is just the opposite of what one would expect for the surface defect lines of the planar bipolar structure, which are almost parallel to the equatorial circle when crossing it [see Fig. 1(c)]. This discrepancy is corrected in the third regime mentioned above ($\epsilon>1$), when there are no closed N^* surfaces; thus no N^* surface is tangential to the droplet surface. With increasing ϵ the planar bipolar structure shows up.

A. Radial ellipsoidal structure with two $s=1$ χ lines

Although the $s=2$ χ defect line in the radial spherical structure tends to be perpendicular to the applied electric field, the metastable orientation parallel to the field exists (see the Appendix) [2]. This metastable orientation is interesting because it can be continuously transformed via ellipsoidal structures into the planar bipolar structure. To achieve this transformation the radial χ line parallel to the electric field must split into two $s=1$ χ lines, each attached to the $s=\frac{1}{2}$ λ line circle, which is formed in the equatorial plane. The process of transformation from radial spherical ($\delta=0$) to planar bipolar structure ($\delta\rightarrow\infty$) via radial ellipsoidal structure with two $s=1$ χ lines ($\mathrm{RES}_{\parallel}$) is illustrated by Figs. 1(a) (initial state), 3 (intermediate states), and 1(c) (final state). A 3D distribution of defect lines and a cross section of the droplets are shown. For low electric field the N^* surfaces are concentric spheres ($\delta=0$) and radial χ line is parallel to the electric field [Fig. 1(a)]. As N^* surfaces become rotational el-

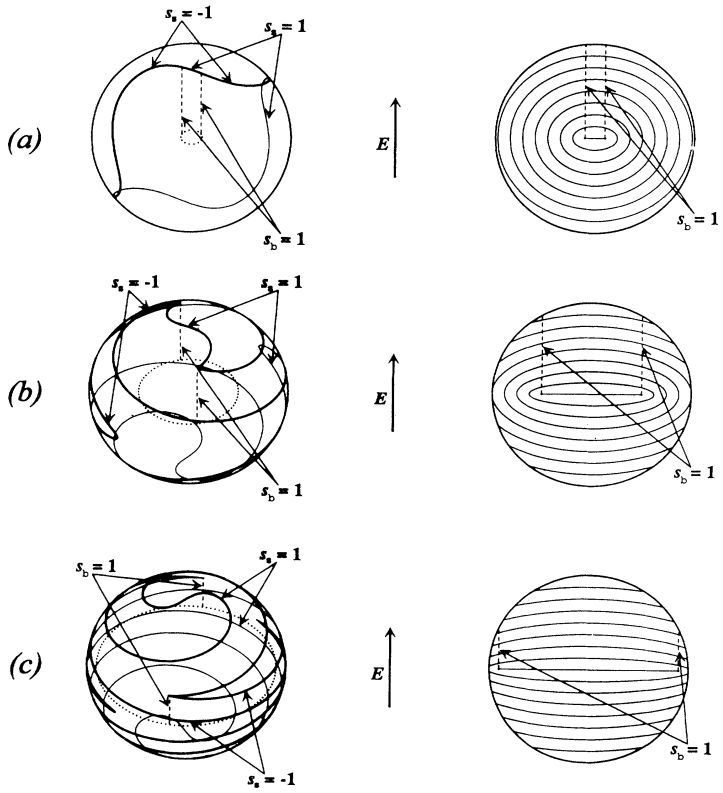

FIG. 3. This figure shows various stages of the evolution of the $RES_{\|}$ when ϵ is increasing. (a) $\epsilon=0.1$, (b) $\epsilon=0.5$, and (c) $\epsilon=0.9$. On the left-hand sketch, the defect lines are shown with the strengths of the χ defect lines—s_b for bulk lines and s_s for surface lines. Surface χ defect lines are drawn with solid lines (hidden lines are thinner), bulk χ defect lines with dashed lines, and λ defect line circle with dotted line. On the right-hand sketch, the cross section of the droplet is shown. The N^* surfaces are represented by solid lines and bulk defect lines by dashed lines. Figures 4–6 are similar to this figure; they describe other ellipsoidal structures.

lipsoids ($\delta>0$), a λ line circle perpendicular to the electric field starts to grow at the droplet center and the surface χ lines start to spiral on the droplet surface. There are three regions with different defect configuration.

(1) $0<r\leq R-\delta$: In this region, the N^* surfaces are closed. Equation (3) is valid and there are just two straight bulk $s=1$ χ lines in the upper half of the droplet. The distance between these two lines is 2δ.

(2) $R-\delta<r\leq r(\delta)$ with $r(\delta)$ given by Eq. (6): In this region, the N^* surfaces are caps of the rotational ellipsoids. On the upper half of the droplet there are still two bulk $s=1$ χ lines but there are also two additional $s=-\frac{1}{2}$ bulk χ lines or two additional surface $s=-1$ χ lines. Hereafter, only the notation of surface defect lines will be used. These additional defect lines are needed to satisfy Eq. (4). On the lower half of the droplet two surface $s=1$ χ lines suffice. Both surface defect lines are spirals.

(3) $r(\delta)<r\leq R$: In this region, the N^* surfaces are caps of rotational ellipsoids but there are no more straight bulk $s=1$ χ lines and two surface $s=1$ χ spirals suffice.

Figure 3 shows defect configuration for three different values of ϵ. In the lower half of the droplet the second and the third regions have the same defect configuration on each N^* cap, because there are no bulk defect lines there. On the other hand, the second region on the upper half of the droplet is easy to recognize in Fig. 3, since the pair of surface $s=-1$ χ defect lines spirals in a different

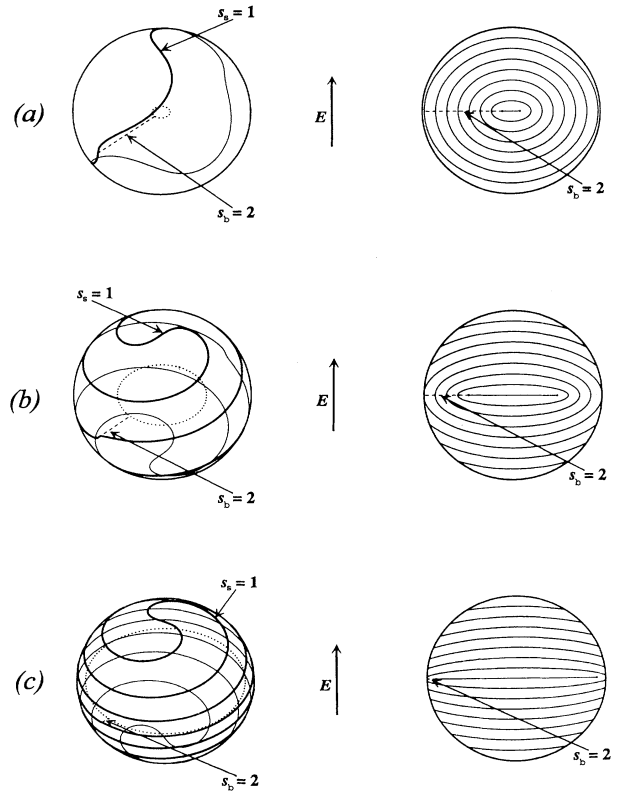

FIG. 4. Similar to Fig. 3, but for the $RES_{\perp}$. (a) $\epsilon=0.1$, (b) $\epsilon=0.5$, and (c) $\epsilon=0.9$.

way than the surface $s=1$ χ defect lines.

The length of the bulk $s=1$ χ lines is $R\sqrt{1-\epsilon^2}$ and as expected these lines get shorter with increasing ϵ. Both ($s=1$ and -1) surface defect lines contribute the same free energy per unit length. The total length of all spirals is relevant to the surface contribution to the free energy. This length increases with the number of turns that the spirals make. The spirals on the surface of the droplet are caused by the rotation of the director fields on the ellipsoidal N^* caps, which are present in the region $R-\delta<r<R$; thus the number of turns each spiral makes on one half of the droplet equals

$$m=\frac{\delta}{(\text{pitch})}=\frac{Q\epsilon}{2\pi}\ , \tag{7}$$

where the dimensionless wave number $Q\equiv qR$ is introduced.

In sufficient electric field, the λ circle disappears from the droplet surface as well as the pair of $s=1$ χ lines. This happens when the parameter ϵ reaches a value of 1. For even higher electric field the regime $\epsilon>1$ is reached and the planar bipolar structure shows up.

B. Radial ellipsoidal structure with a tilted $s=2$ χ line

When the $s=2$ χ defect line in the radial spherical structure is perpendicular to the low electric field, the following transformation from radial spherical ($\delta=0$) to planar bipolar structure ($\delta\to\infty$) via radial ellipsoidal structure with a tilted $s=2$ χ line ($\text{RES}_\perp$) illustrated in Figs. 1(a) (initial state), 4 (intermediate states), and 1(c) (final state), is expected. The electric field in Fig. 1(a) is perpendicular to the $s=2$ χ line. The λ defect line circle is formed in the equatorial plane. The bulk $s=2$ χ defect line, which is attached to it, lies only in the first region ($0<r<R-\delta$) described in the general discussion on ellipsoidal structures. Since there are no bulk defect lines in the second region of the droplet, the defect configuration on N^* caps in the second and the third region are the same. There are only two regions with different defect configurations.

(1) $0<r\le R-\delta$: In this region, the N^* surfaces are closed and there is just one bulk $s=2$ χ defect line in the equatorial plane, extending from the λ defect line circle to the droplet surface.

(2) $R-\delta<r\le R$: In this region, the N^* surfaces are caps of the rotational ellipsoids. There is no bulk defect line in this region and a pair of surface $s=1$ χ lines appears. These additional defect lines are needed to satisfy Eq. (4). They spiral from the lower to the upper pole of the droplet (see Fig. 4).

The length of the bulk χ line is $R(1-\epsilon)$ and decreases with increasing electric field. The surface χ lines are similar to the surface defect lines in the droplet with $\text{RES}_\parallel$. The major difference is the absence of the surface $s=-1$ χ line. The total length of all surface defect lines is the same as for the $\text{RES}_\parallel$. In increasing electric field the surface χ lines wind more and more and the process is accompanied by the relative rotation of the bulk χ line. By comparing Figs. 4(a) and 4(b) the rotation of the bulk χ line with respect to the direction of the surface χ line on the droplet poles is seen. The angle of rotation is equal to the product of the cholesteric wave number q and the change of the length of the bulk χ line, which can be written as

$$q\Delta\delta\ . \tag{8}$$

Further winding of χ line spirals on the droplet surface and rotation of the bulk χ line can be seen in Fig. 4(c). The λ line circle is already of almost the same radius as the droplet. In sufficient electric field, the λ circle disappears on the droplet surface as well as the bulk $s=2$ χ line. This happens when the parameter ϵ reaches a value of 1. For even higher electric field, the regime $\epsilon>1$ is reached and the planar bipolar structure shows up.

There are some vaguenesses about the director field on the N^* surfaces near the border of the first and second regions of the droplet. Although the topological constraints expressed by Eqs. (3) and (4) are satisfied, the director field on the closed N^* surface with $r=R-\delta$ is far from being similar to the director field on the N^* cap with the same r. This would lead to a defect surface on the ellipsoid between the two regions, which is certainly unstable [3]. There are several possibilities for overcoming this situation. One possibility is a single surface $s=2$ χ spiral which leads to planar monopolar structure. This structure has, however, higher free energy than the planar bipolar structure [15] and at some point must transform into the latter. Another possibility is that the director field on the closed N^* surfaces near the border between the two regions be deformed in order to achieve a continuous director field when crossing the border $r=R-\delta$. How exactly this is done and how it effects the free energy is difficult to predict and will be left out of the present discussion.

C. Diametrical ellipsoidal structure with two $s=\frac{1}{2}$ χ lines

The bulk $s=1$ χ defect line in the diametrical spherical structure tends to be parallel to an applied low electric field. When the field is increased sufficiently, the bulk $s=1$ χ line is expected to split into two bulk $s=\frac{1}{2}$ χ lines, both being parallel to the applied field, and the λ defect line circle is created in the equatorial plane [see Figs. 1(b) (initial state), 5 (intermediate states), and 1(c) (final state)]. The diametrical ellipsoidal structure with two $s=\frac{1}{2}$ χ lines ($\text{DES}_\parallel$) is similar to the $\text{RES}_\parallel$. There are again three different regions concerning defects.

(1) $0<r\le R-\delta$: In this region, the N^* surfaces are closed and there are just two straight bulk $s=\frac{1}{2}$ χ lines needed to satisfy Eq. (3). The difference with respect to the radial ellipsoidal structure with two $s=1$ χ lines is that in the case of $\text{DES}_\parallel$ the χ lines extend into the upper as well as into the lower half of the droplet.

(2) $R-\delta<r\le r(\delta)$ with $r(\delta)$ given by Eq. (6): In this region, the N^* surfaces are caps of the rotational ellipsoids. There are still two bulk $s=\frac{1}{2}$ χ lines but according to Eq. (4) there is no need for additional χ lines. So the

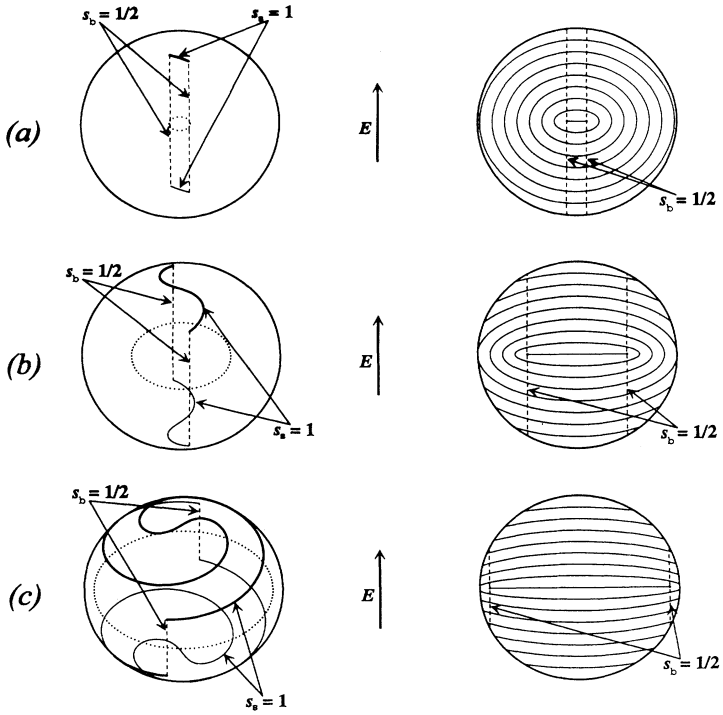

FIG. 5. Similar to Figs. 3 and 4. It shows the evolution of the $DES_{\parallel}$. (a) $\epsilon=0.1$, (b) $\epsilon=0.5$, and (c) $\epsilon=0.9$.

situation concerning defect lines in this region is unchanged compared to the first region described above.

(3) $r(\delta)<r\leq R$: In this region, the N^* surfaces are caps of rotational ellipsoids but there are no more straight bulk $s=1$ χ lines and two surface $s=1$ χ spirals suffice.

The length of the bulk $s=\frac{1}{2}$ χ line is $l=2R\sqrt{1-\epsilon^2}$. The length of the surface χ spirals is here smaller than in the case of the droplets with radial ellipsoidal structures, because they do not extend from the equator to the poles. But with increasing ϵ their lengths increase and at $\epsilon=1$ the λ circle disappears from the droplet surface as well as the bulk $s=\frac{1}{2}$ χ lines. For even higher electric field the regime $\epsilon>1$ is reached and the planar bipolar structure shows up.

D. Diametrical ellipsoidal structure with tilted $s=1$ χ line

Besides the above stable orientation of the diametrical χ line, there is a metastable orientation of the diametrical $s=1$ χ defect line perpendicular to the applied electric field. With the appearance of the ellipsoidal structures at intermediate electric fields, the diametrical χ line lying in the equatorial plane splits at the center of the droplet. The λ defect line circle that is created in the equatorial plane connects the two parts of the χ line [see Fig. 6(a)]. The transition from diametrical spherical ($\delta=0$) to planar bipolar structure ($\delta\rightarrow\infty$) via diametrical ellipsoidal structure with tilted $s=1$ χ lines ($DES_{\perp}$) is illustrated in Figs. 1(b) (initial state), 6 (intermediate states), and 1(c) (final state). Here one must imagine that the electric field in Fig. 1(b) lies perpendicular to the χ defect line. The diametrical ellipsoidal structure with tilted $s=1$ χ lines is similar to the $RES_{\perp}$. But there are no problems with the continuity of the director field on the N^* surfaces that are lying near the border between the first and the second regions introduced in the general discussion on ellipsoidal

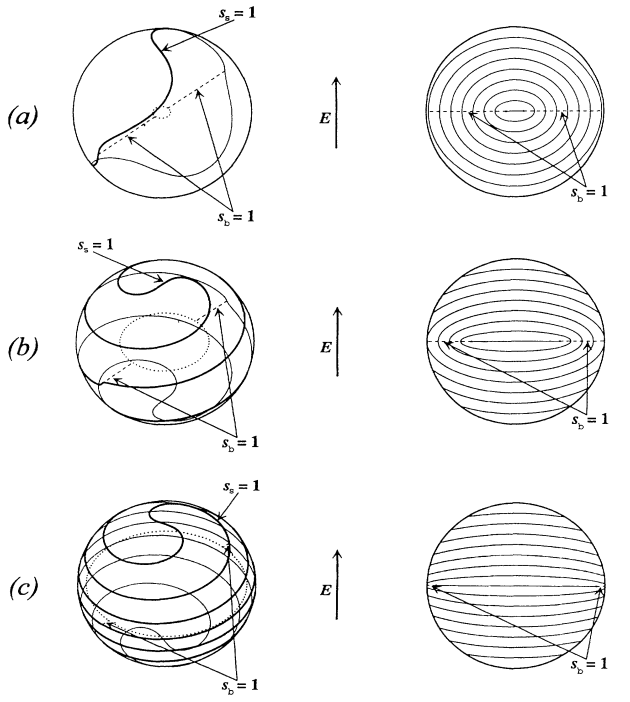

FIG. 6. Similar to the three previous figures, but for the $DES_{\perp}$. (a) $\epsilon=0.1$, (b) $\epsilon=0.5$, and (c) $\epsilon=0.9$.

structures. As in the case of $RES_\perp$ the defect configuration on the N^* surfaces in the second and in the third regions is the same and there are only two different regions involving defects.

(1) $0<r\leq R-\delta$: In this region, the N^* surfaces are closed and there are just two bulk $s=1$ χ defect lines in the equatorial plane, extending diametrically from the λ defect line circle to the droplet surface [Fig. 6(a)]. The difference with respect to the $RES_\perp$ is that in the case of $DES_\perp$ there are two bulk $s=1$ χ lines instead of one bulk $s=2$ χ line.

(2) $R-\delta<r\leq R$: In this region, the N^* surfaces are caps of the rotational ellipsoids. There is no bulk defect line in this region and a pair of surface $s=1$ χ lines appears. These additional defect lines are needed to satisfy Eq. (4). They spiral from the lower to the upper pole of the droplet (see Fig. 6) and are the same as those in droplets with radial ellipsoidal structure with a tilted $s=2$ χ line.

The length of one bulk $s=1$ χ line is $l=R(1-\epsilon)$. The total length of all surface defect lines is the same as for the $RES_\perp$, as their shape is equal.

In sufficient electric field, the λ circle disappears from the droplet surface as well as the bulk $s=1$ χ lines ($\epsilon=1$). For even higher electric field the regime $\epsilon>1$ is reached and the planar bipolar structure shows up.

IV. THE FREE ENERGY

Once we have a geometrical model for the shape of N^* surfaces and asymmetry allowed combinations of disclination lines, the corresponding free energy must be estimated to enable us to find the most stable structure. Elastic and field contributions will be considered. The following typical material constants will be used: average Frank elastic constant $K=5\times10^{-12}$ N, cholesteric pitch $2\pi/q=0.5$ μm, and dielectric anisotropy $\varepsilon_a=-5$.

A. Elastic free energy

The dominant part of the free energy associated with the deformation of the N^* structure is concentrated in the vicinity of the singular and nonsingular χ lines [10]. Using a single elastic constant approximation the elastic free energy density at a distance r from the core of the defect line with the strength s can be written as

$$f=\frac{1}{2}K\frac{s^2}{r^2}\ . \tag{9}$$

Neglecting details of the shapes of the lines and the interference between different lines, we simply assume that the contribution of each line defect to the free energy is obtained by the integration of f over an effective volume. A cylinder with the length equal to the length of the disclination line and the radius equal to the droplet radius R will be used as such an effective volume. For the bulk defect lines these are full cylinders while for the surface defect lines these are only half cylinders. The cores of the cylinders, where the divergent elastic free energy density (9) surpasses the difference between the free energy of the bulk N^* and isotropic phase Δf must be excluded. An estimate for the radius of the core $r_c^s=s\sqrt{K/a\Delta T}/S$ is obtained after comparing the free energy density (9) to the first term of the Landau free energy expansion $\frac{1}{2}\Delta TaS^2$ [3,10]. With $\Delta T=5$ K, $S=0.4$, and $a=10^5$ J/K M^3 one finds $r_c^1=8$ nm. For all further calculations the radius of a core of χ defect line with strength 1 will be taken to be $r_c^1=10$ nm. Therefore, in supramicrometer size droplets $R\gg r_c^s$ one can neglect the contribution of the free energy of the cores and approximately write the elastic free energy as a sum of bulk and surface (boundary) defect lines contributions,

$$F_{\rm el}=K\pi\left[\sum_{\rm bulk}l_i s_i^2\ln\frac{R}{r_c^{s_i}}+\frac{1}{2}\sum_{\rm surface}l_j s_j^2\ln\frac{R}{r_c^{s_j}}\right]\ . \tag{10}$$

l_i stands for the length of the ith bulk χ defect line and l_j for the length of the jth surface χ defect line. As we mentioned above λ lines are nonsingular in the director field and thus have no significant contribution to the elastic free energy.

The approximation of the spherical volume with the cylinder was tested on spherical structures using the solutions (1). The results are in good agreement with the approximate free energy given by (10) [10]. It is, on the other hand, hard to imagine that the cylindrical volume (with radius R) will give reasonable results for the surface χ defect lines that make many turns when spiraling from the upper to the lower pole of the droplet. A lucky circumstance that the radius of the cylinder enters the expression for the free energy (10) in a logarithm allows us to use the droplet radius R as the radius of the cylinder that encircles a surface χ defect line. Anyhow, the length of the χ defect spirals must be calculated. The length of one spiral that makes m turns on one half of the droplet equals

$$l=2R\int_0^{\pi/2}\sqrt{4\pi^2m^2\cos^4t+1}\,dt\ . \tag{11}$$

In the limit $m>10$ Eq. (11) can be within 4% accuracy approximately as

$$l=\pi^2Rm\ . \tag{12}$$

B. Electric free energy

This contribution is usually written in terms of the coupling of electric and director fields

$$f_{\rm field}=-\tfrac{1}{2}\varepsilon_0\varepsilon_a(\vec{n}\cdot\vec{E})^2\ , \tag{13}$$

where ε_a is the anisotropy of the dielectric tensor [3].

1. Low electric field

Negative anisotropy of the dielectric tensor favors perpendicular orientation of the director in the electric field. To see how a weak electric field with $R<\xi_E=\sqrt{K/\varepsilon_0|\varepsilon_a|E^2}$ (ξ_E is the electric coherence length [17]) affects a spherical structure, we assume that N^* surfaces remain spherical. Taking solutions (1) we find (in a

limit where droplet radius is much bigger than the cholesteric pitch—$Rq = Q \gg 1$) that the integration of the f_{field} over the droplet yields an orientation-independent contribution

$$F_0 = -\frac{1}{6}\varepsilon_0\varepsilon_a \frac{4\pi}{3} R^3 E^2 \ . \tag{14}$$

This result was obtained using zeroth-order terms only. A more detailed calculation is given in the Appendix. The relative magnitude of higher-order contributions (which depend on relative orientation of χ lines with respect to the electric field) turns out to be Q^{-1} at most. Since the elastic part of the total free energy is calculated approximately, for the electric part the zeroth-order terms (14) will suffice. Higher-order terms will be taken into account only to determine the preferable orientation of the χ defect lines in low electric field, as is shown in the Appendix.

The $s=1$ χ defect line in a droplet with diametrical spherical structure tends to be parallel to the electric field [see Fig. 7(a)], while the $s=2$ χ defect line in a droplet with radial spherical structure tends to be perpendicular to the electric field [see Fig. 7(b)]. Besides these two stable orientations there are two metastable ones. The metastable orientation of the $s=1$ χ defect line in a droplet with a diametrical spherical structure is perpendicular to the electric field. The metastable orientation of the $s=2$ χ defect line in a droplet with a radial spherical structure is parallel to the electrical field. See the Appendix and Fig. 7 for further information. The contribution of the escaped cores to the electric part of the free energy in these structures is of the second order in Q^{-1} and thus has no significant influence on the orientational dependence of χ lines. Nevertheless, it should be kept in mind that escaped cores tend to be perpendicular to the field.

2. *Intermediate and high electric fields*

Calculation of the electric part of the free energy in higher electric fields can approximately be estimated in the limit $Q \gg 1$. Formally, a function $g(\epsilon)$ is introduced as the ratio between the actual electric free energy and the electric free energy of spherical structures (14); $g(\epsilon) \equiv F_{\text{field}}/F_0$. So $g(0)=1$ and $g(\infty)=0$, because the planar structures ($\epsilon \to \infty$) have zero electric free energy. To calculate $g(\epsilon)$ in the limit $Q \gg 1$ expression (13) is averaged along $\vec{q}$ over one period $2\pi/q$. This averaging yields

$$\langle -\tfrac{1}{2}\varepsilon_0\varepsilon_a(\vec{n}\cdot\vec{E})^2 \rangle = -\tfrac{1}{4}\varepsilon_0\varepsilon_a E^2 \sin^2\theta \ , \tag{15}$$

where θ is the angle between $\vec{q}$ and $\vec{E}$. Integrating (15) over the droplet gives the electric free energy. Since $g(\epsilon)$ is normalized to 1 for spherical structures and the average of $\sin^2\theta$ for spherical structures gives $\frac{2}{3}$, the function $g(\epsilon)$ takes the form

$$g(\epsilon) = \frac{3}{2}\frac{1}{R^3}\int_0^R \int_0^{\rho(z)} \sin^2\theta(\rho,z)\rho \, d\rho \, dz \ , \tag{16}$$

where θ is in fact the local value of the angle between the normal to the N^* surface ($\vec{q}$) defined by (2) and the external field $\vec{E}$. The electric free energy of ellipsoidal structures can now be written as

$$F_{\text{field}} = -\frac{1}{6}\varepsilon_0\varepsilon_a \frac{4\pi}{3} R^3 E^2 g(\epsilon) = F_0 g(\epsilon) \ . \tag{17}$$

In the next section this contribution to the free energy will be combined with the elastic part and then used for the determination of the particular stable structures.

C. Simplified total free energy

In order to eliminate the quantities that are not really important and to get a better physical feeling for the relative importance of the particular terms in the total free energy the dimensionless quantities are introduced,

$$\mathcal{F} \equiv \frac{F}{\pi K R} \ , \quad e \equiv \frac{E}{E_0} \ , \quad X^{-1} \equiv \frac{r_c^1}{R} \ , \quad L_i \equiv \frac{l_i}{R} \ . \tag{18}$$

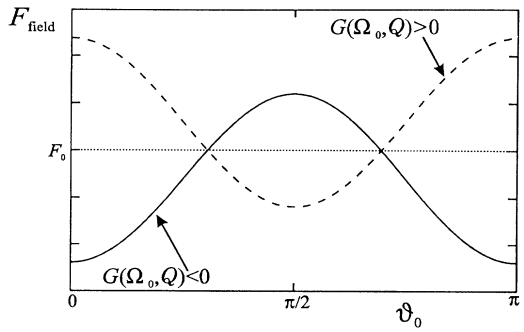

(a)

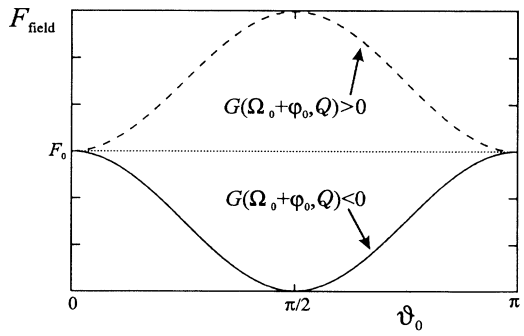

(b)

FIG. 7. Corrections to the zeroth-order electric free energy show orientational dependence of the spherical structures: (a) diametrical spherical and (b) radial spherical structure. Solid lines correspond to the stable orientations and dashed lines to the metastable orientations of the spherical structures in low electric field. In the case of DSS, the parallel orientation of the diametrical $s=1$ χ line is stable and the perpendicular one is metastable. In the case of RSS, the perpendicular orientation of the radial $s=2$ χ line is stable and the parallel orientation is metastable. The angle on the abscissa is between the electric field and the χ line. For details see the Appendix and Eqs. (A2), (A3), and (A5).

Everything is somehow normalized on the droplet size. The electric field E_0 corresponds to the condition $\xi_E = R = \sqrt{K/\varepsilon_0|\varepsilon_a|E_0^2}$. To compare contributions of geometrical constraints and electric field we choose $R = 10\ \mu m$ ($X = 1000$) and get $E_0 = 0.0336\ V/\mu m$. The dimensionless free energy of a $s = 1$ χ line that is $l = R$ long is thus

$$a = \ln X \approx 6.9 \ . \tag{19}$$

The electric contribution (17) to the free energy now reads

$$\mathcal{F}_{\text{field}} = be^2 g(\epsilon) \ ,$$
$$b = -\frac{1}{6}\varepsilon_0\varepsilon_a E_0^2 \frac{4\pi}{3} R^3 \frac{1}{\pi K R} \approx 0.22 \ . \tag{20}$$

The total dimensionless free energy is the sum of the elastic (10) and electric (20) contributions:

$$\mathcal{F} = a\left[\sum_{\text{bulk}} L_i s_i^2 + \tfrac{1}{2}\sum_{\text{surface}} L_j s_j^2\right] + be^2 g(\epsilon) \ . \tag{21}$$

Using the fact that r_c^s enters the elastic free energy in logarithm in expression (21) the difference between core radii [10] is neglected.

The free energy of radial and diametrical ellipsoidal structures can be estimated using expression (21). In our calculations, the χ line spirals are treated as $s = 1$ surface χ defect lines [16] and other possibilities are left for discussion in the concluding section.

The parameter describing the transition from spherical to planar bipolar structure, via ellipsoidal structures, is $\epsilon = \delta/R$. Substituting $\epsilon = 0$ in the expressions for ellipsoidal structures, the expressions for spherical structures are obtained (see Table I). Similarly, substituting $\epsilon = 1$ in the expressions for ellipsoidal structures the expressions for planar bipolar structure are obtained. So we neglect the minute difference between ellipsoidal structures and the PBS for $\epsilon > 1$ [compare the middle of Fig. 1(c) with Fig. 2(b)]. All N^* surfaces are at this point slightly deformed circles as can be seen from Fig. 2(b). Although the exact director configuration at this point is not known, it is plausible that a very small amount of energy (if any) is needed to flatten deformed N^* surfaces and thereby achieve the exact planar bipolar structure.

In Table I, the expressions for total free energy of droplets with structures of interest are collected. Particular contributions (bulk, surface, electric) are shown separately to get a better overview of the characteristics of the individual structure. The free energy $\mathcal{F}_{\text{el}}^{\text{surface}}$ of the surface χ lines is calculated with Eq. (21), using Eqs. (7) and (12) to estimate the length of the surface χ lines. This estimation gets better with increasing ϵ and Q. It is difficult to calculate the function $g(\epsilon)$ from Eq. (16). Therefore, its value is estimated with the following approximation. A droplet is separated into two regions, a region cut out of the droplet by the surface of a cylinder with radius δ and the rest of the droplet. The symmetry axis of the cylinder is parallel to the electric field. To obtain $g(\epsilon)$, the director field inside the cylinder is taken to be normal to the electric field, so the electric free energy of this region is neglected. The average electric free energy density of the rest of the droplet is supposed to be the same as that of the spherical structures. The function $g(\epsilon)$ calculated in this way is the ratio between the volume, cut off by the cylinder, and the volume of the droplet.

The free energies for different structures given in Table I are used to construct the stability diagram [see Figs. 8(a) and 8(b)]. Therefore, the free energy at certain electric fields must be minimized with respect to the parameter ϵ. This minimization leads to the results presented in Figs. 9(a) and 9(b). The first one shows ϵ as a function of electric field for $Q = 40\pi$ and the second one the free energy as a function of electric field for different structures with $Q = 40\pi$.

TABLE I. Different contributions to the total free energy for droplet with various structures in electric field. The total energy for each structure is a sum of all three contributions—bulk defect lines, surface defect lines, and field. The spherical structures do not have surface defect lines, while the planar bipolar structure has only surface defect lines and also zero electric field contribution.

Structure	$\mathcal{F}_{\text{el}}^{\text{bulk}}$	$\mathcal{F}_{\text{el}}^{\text{surface}}$	$\mathcal{F}_{\text{field}}$
DSS	$2a$	0	$\frac{1}{2}be^2$
RSS	$4a$	0	$\frac{1}{2}be^2$
$\text{DES}_{\parallel}$	$2a\sqrt{1-\epsilon^2}$	$\frac{\pi}{2}aQ(1-\sqrt{1-\epsilon^2})$	$\frac{1}{2}be^2(1-\epsilon^2)^{3/2}$
$\text{RES}_{\parallel}$	$4a\sqrt{1-\epsilon^2}$	$\frac{\pi}{2}aQ\epsilon$	$\frac{1}{2}be^2(1-\epsilon^2)^{3/2}$
$\text{DES}_{\perp}$	$2a(1-\epsilon)$	$\frac{\pi}{2}aQ\epsilon$	$\frac{1}{2}be^2(1-\epsilon^2)^{3/2}$
$\text{RES}_{\perp}$	$4a(1-\epsilon)$	$\frac{\pi}{2}aQ\epsilon$	$\frac{1}{2}be^2(1-\epsilon^2)^{3/2}$
PBS	0	$\frac{\pi}{2}aQ$	0

V. DISCUSSION

The first step in obtaining the ellipsoidal structures in N^* droplets was to assume rotational ellipsoids as intermediate N^* surfaces (cholesteric surfaces) between concentric spheres in spherical structures and planes in planar structures. The second step is to use Eqs. (3) and (4) to find possible defect combinations for 2D nematic director field on these N^* surfaces. Since the observations of N^* droplets perpendicularly to the electric field reasonably well confirm this assumption, a detailed discussion of ellipsoidal structures was considered interesting.

In zero electric field radial spherical structure (RSS) and sometimes also diametrical spherical structure (DSS) are stable and for high electric fields planar structures are stable [1,2]. In this contribution we propose radial ellipsoidal and diametrical ellipsoidal structures as intermediate structures for intermediate electric fields. Two of them are particularly interesting.

The first one is the radial ellipsoidal structure with a tilted $s = 2$ χ line, which is observed experimentally. Our

model qualitatively explains most of the observed static features [2,6], although some uncertainties remain.

(1) Our theoretical calculations show that the radial χ line tilts into a position perpendicular to the electric field and the experiments confirm this prediction [2,6].

(2) In intermediate electric field a circle is created at the droplet center (the $s=\frac{1}{2}$ λ defect line). This circle grows with increasing electric field and finally disappears. This is observed experimentally as well [2,6], although the creation of the circle is continuous in experiments, while our estimates for RSS$\rightarrow$RES$_\perp$ transition [Table I and Fig. 9(a)] show a jump in the radius δ of the circle. Furthermore, measured δ increases in small steps, which is beyond our approximation.

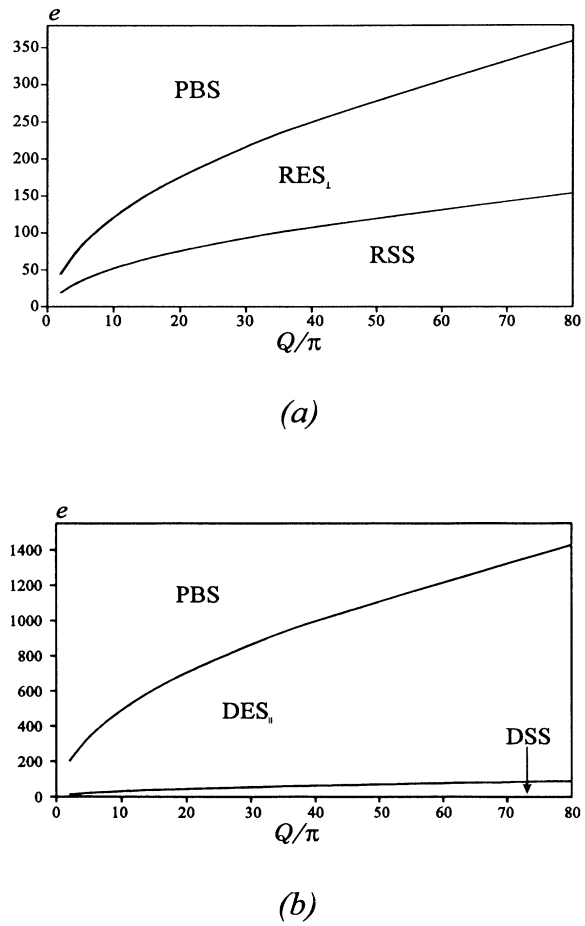

FIG. 8. The stability diagrams for radial (a) and diametrical (b) structure. The lines are separating stability regions of planar bipolar structure (PBS), radial ellipsoidal structure with a tilted $s=2$ χ line (RES$_\perp$) and radial spherical structure (RSS) in case (a) and planar bipolar structure (PBS), diametrical ellipsoidal structure with two $s=\frac{1}{2}$ χ lines (DES$_\parallel$) and diametrical spherical structure (DSS) in case (b). The transition lines are not drawn for very small Q, because our calculations are valid in the approximation $Q\gg1$. The relation between threshold electric field and the pitch $q/2\pi$ is in good qualitative agreement with the experiments [2].

(3) The director field on N^* surfaces is not yet predicted. We have an idea of how it looks on the closed N^* surfaces and on the N^* caps that are not close to the limiting N^* surface with $r=R-\delta$. In the region near the N^* surface with $r=R-\delta$ the director field should continuously transform in order to connect the two types of director configurations. How this happens remains an open question.

(4) The rotation of the bulk $s=2$ χ line was observed and our model provides a reasonable explanation [see Eq. (8) and the text above it].

There is a slight difference between the transition described above and the observed transition for a larger pitch [2]. In the case of larger pitch the radial χ line does not rotate in the plane perpendicular to the electric field. At the same time the pitch decreases in this plane and the circle grows. In the frame of our model structures this can be restated as follows: no additional rotational ellipsoids are cut into two caps by the droplet surface; there-

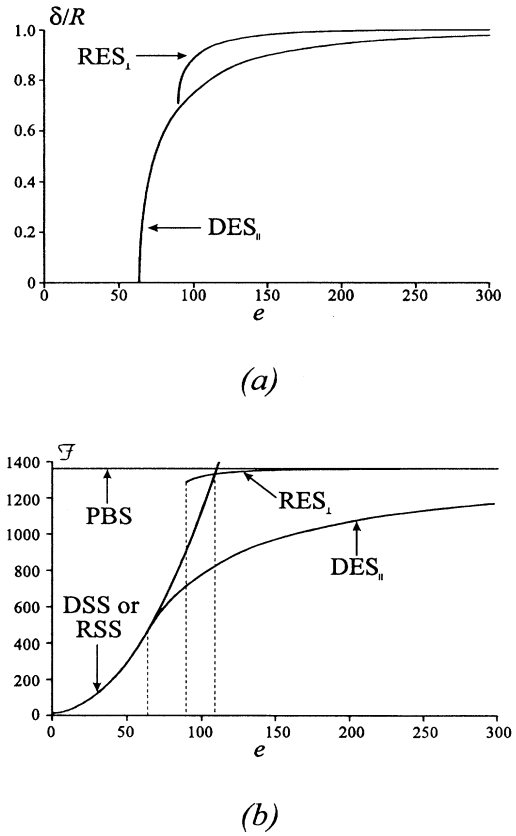

FIG. 9. (a) Dependence of the parameter $\epsilon=\delta/R$ on electric field is shown for the two most interesting ellipsoidal structures RES$_\perp$ and DES$_\parallel$. (b) Total free energy $\mathcal{F}$ for several structures is shown as the function of electric field. The difference between the free energies of DSS and RSS is neglected, since the elastic free energy is comparable to the electric free energy only for very low electric field. Otherwise it is negligible and the electric part prevails. In both figures the dimensionless wave number is $Q=40\pi$.

fore, Eq. (8) does not change and the radial χ line does not have to rotate.

The second particularly interesting structure is the diametrical ellipsoidal structure with two $s=\frac{1}{2}$ χ lines. It is interesting because it has the lowest free energy [see Fig. 9(b)]. Further, it shows a continuous growth of the λ circle from 0 to R. The most significant difference compared to other ellipsoidal structures in the length of the surface $s=1$ χ defect lines for small ϵ [see Figs. (3)–(6)]. The dependence of ϵ on the electric field for this structure is in good qualitative agreement with experimental results for the radial ellipsoidal structure with a tilted $s=2$ χ line [see Fig. 9(a) and Fig. 3 in Ref. 6], although the quantitative results still differ significantly. This structure has not yet been observed, probably because the diametrical spherical structure is rarely observed.

The relaxation of a planar bipolar structure, observed when large electric field is abruptly switched off to a zero electric field [6], can be qualitatively explained with a structure which originates from the diametrical ellipsoidal structure with two $s=\frac{1}{2}$ χ lines. An abrupt switchoff may throw the director field from the metastable PBS-RES$_{\perp}$-RSS line to the stable DES$_{\parallel}$-DSS line [Fig. 9(b)]. This change of director configuration happens in a cascade of metastable structures, "characterized by several stacked disclination rings parallel to, but not in, the equatorial plane" [6]. The additional λ circles are a result of recombination of near N^* planes into many rotational ellipsoids like N^* surfaces. So the N^* surfaces in this metastable structures are mainly closed and similar to the N^* surfaces in the region $r+\delta<R$ in the ellipsoidal structures. At the center of each of these rotational ellipsoids like N^* surfaces there is a $s=\frac{1}{2}$ λ line circle and these rotational ellipsoids like N^* surfaces are separated by $s=-\frac{1}{2}$ λ line circles. Therefore, there must be $n+1$ $s=\frac{1}{2}$ λ line circles separated by n $s=-\frac{1}{2}$ λ line circles. All λ line circles are connected by a pair of $s=\frac{1}{2}$ χ lines passing through them. The pair is similar to the one in diametrical ellipsoidal structure with two $s=\frac{1}{2}$ χ lines, although the dependence of the distance between the two lines on electric field is probably different. The λ line circles eventually pairwise recombine (one $s=\frac{1}{2}$ and one $s=-\frac{1}{2}$) leaving only one $s=\frac{1}{2}$ λ line circle at the droplet center and a pair of χ lines. The resulting structure is a diametrical ellipsoidal structure with two $s=\frac{1}{2}$ χ lines.

Pros and cons

A general conclusion can be made from the above discussion. The qualitative features of our models of ellipsoidal structures are in good agreement with the experimental observations [1,2,6]. This strongly supports the proposed ellipsoidal structures. On the other hand, the quantitative features show considerable deviations compared to the experiments. For example, the predicted threshold field strengths are about 10 times higher than the observed [6]. The discrepancy gets smaller with increasing field but does not vanish even in very high fields. This and also some other differences mentioned above can be explained.

The main reason for the quantitative differences is, in our opinion, the elastic free energy of the planar bipolar structure which might be greatly overestimated. Our calculations show that it is about 70 times higher than the elastic free energy of the spherical structures of $Q=40\pi$. It is difficult to imagine that two director configurations which are not so very different will have such different elastic free energy. The explanation lies in the assumptions we made.

First of all, we have assumed nondegenerate N^* surfaces. If this assumption is relaxed then the χ defect lines with integer strength can have escaped cores [16], which lowers the elastic free energy. This is in agreement with the experimental fact that the surface χ spirals were not observed. Second, the assumption of the strong planar anchoring is also questionable. The weak anchoring on the liquid crystal to polymer interface could substantially lower the elastic free energy, since there could be many fewer defects on the surface of the droplet. If, for example, the weak anchoring of the usual Rapini-Papoular [18] form

$$f_s=\tfrac{1}{2}W_0\sin^2\Theta\ , \tag{22}$$

where Θ is the angle between the preferred and the actual director orientation, is supposed and the intrinsic bulk N^* configuration is taken in the entire droplet, the free energy is just the surface energy

$$\mathcal{F}_s=\frac{2}{2}\frac{RW_0}{K}\ . \tag{23}$$

For the $W_0=2\times10^{-4}$ J/m^2 [19,20] this yields $\mathcal{F}_s=270$, which is about 5 times less than our estimation for the strong anchoring. Any other structure on the N^* surfaces will naturally appear only if it lowers the free energy still further so that this is the upper limit for the free energy of the planar bipolar structure. The elastic free energy of the spherical structures does not change. It is clear from Fig. 9(b) that decreasing the free energy of the planar bipolar structure leads to the lower threshold values of the electric field.

Another problem is the local electric field within the droplet. Taking it constant and equal to the applied electric field is a very crude estimate. Even for nonchiral nematic droplets with very simple configurations the local electric fields can vary a lot [21]. For a more detailed structure study a more accurate calculation of the local electric field is certainly needed.

A closer inspection of microphotographs of chiral nematic droplets in Fig. 2(b) in Kitzerow and Crooker [6] shows that the N^* surfaces are made of two parallel circles and a part of torus rather than ellipsoids. The difference between our model and actual N^* surfaces is the most obvious for very flat ellipsoids—the one with short axis r much shorter than the long axis $r+\delta$. We plan to include this nonellipsoid ansatz for N^* surfaces in our numerical simulation of the director field.

The above considerations indicate that, in general, the proposed models are correct. More realistic boundary conditions and numerical simulation of the director field will hopefully give quantitative agreement with the exper-

iments. This is the direction in which our further investigations are oriented.

APPENDIX: SPHERICAL STRUCTURES IN LOW ELECTRIC FIELD

Electric contribution to the free energy of spherical structures can be derived analytically if nondegenerated N^* surfaces are assumed. The electric free energy density (13) is defined everywhere except in the points where director $\vec{n}$ is singular and, furthermore, its value outside this point is always finite. The total electric free energy can thus be integrated over the droplet using the solutions (1) in the entire droplet. By doing so a negligible error is made when conditions $Rq=Q\gg 1$ and $R/r_c^1\gg 1$ are fulfilled, since the isotropic phase inside the core is taken to be the N^* phase.

To perform the integration of the electric free energy the spherical coordinate system is used, so that the z axis coincides with the radial χ line of strength s [as in Eqs. (1)]. Let the direction of the electric field $\vec{E}$ be described by angles ϑ_0 (azimuthal angle) and φ_0 (polar angle). We described the simple director configurations in spherical structures as

$$\vec{n}=\cos\Omega\vec{e}_\vartheta+\sin\Omega\vec{e}_\varphi\ ,\quad \Omega=(s-1)\varphi+qr+\Omega_0\ . \tag{A1}$$

Equation (24) yields the total electric free energy F_{field} of RSS and DSS cases

$$F_{s=2}=F_0[1+\tfrac{3}{8}\sin^2\vartheta_0 G(\Omega_0+\varphi_0,Q)]\ , \tag{A2}$$

$$F_{s=1}=F_0[1+\tfrac{3}{4}(1-\tfrac{3}{2}\sin^2\vartheta_0)G(\Omega_0,Q)]\ , \tag{A3}$$

with

$$G(u,Q)=\frac{1}{Q^3}\sin 2u+\frac{2}{Q^2}\cos(2u+2Q)+\left[\frac{2}{Q}-\frac{1}{Q^3}\right]\sin(2u+2Q)\ . \tag{A4}$$

In the limit $Q\gg 1$ the shape of $G(u,Q)$ can approximately be described by the first-order term in $1/Q$:

$$G(u,Q)\approx\frac{2}{Q}\sin(2u+2Q)\ . \tag{A5}$$

Figure 7 shows the dependence of the electric free energy on the orientation of the χ lines in the electric field.

1. Diametrical spherical structure

A droplet with DSS is cylindrically symmetric about the z axis and that is why the polar angle φ_0 has no influence on the electric free energy $F_{s=1}$. It follows from Eq. (A3) that the angle ϑ_0 between $\vec{E}$ and the direction of the $s=1$ χ line affects $F_{s=1}$. Different orientations between $\vec{E}$ and the χ line, however, cause a relative change of the electric free energy that is of the order Q^{-1} at most. In our calculations R is assumed to be much larger than the pitch $q/2\pi$, for example, $qR=Q=40\pi$, so the changes are in the range of 1%. One more thing can be deduced from Eq. (A3). Function G determines some sort of amplitude of orientational dependence of total electric free energy. For $G=0$ all orientations of the χ line would be equivalent.

The value of G depends on $Q=qR$, which is given by the substance one uses and the size of the droplet and is thus fixed for a particular droplet, and on Ω_0. Neither minimization of the total elastic free energy, nor the tangential boundary conditions constrain Ω_0. In the electric field Ω_0 affects the electric free energy and thus adjusts its value in order to minimize the free energy. If $G>0$ then $\vartheta_0=\pi/2$ gives minimal electric free energy. If, on the other hand, $G<0$ then $\vartheta_0=0$ gives minimal electric free energy [see Fig. 7(a)]. The first minimum is not global so this (perpendicular) orientation is metastable, while the other minimum represents the stable (parallel) orientation. In both cases the lowest minimum of the free energy is reached when G takes its extreme value $\pm 2/Q$ [see Fig. 7(a)].

It is quite illustrative to give the physical reasons for these results. The structures in successive spherical shells, when moving from the center of the droplet, are, respectively, . . . , bipolar, twisted bipolar, concentric, twisted bipolar, bipolar, twisted bipolar, concentric, . . . and so on [10,15]. The spherical shells with the same structure have increasingly larger radius, the increment being $\frac{1}{2}$ of the pitch π/q [see Fig. 1(b)]. Calculation of electric free energy of thin spherical shells with particular structures shows that concentric structure has zero electric free energy because $\vec{n}$ is everywhere perpendicular to the electric field ($\vec{E}$ is parallel to the χ line) and the bipolar structure has maximum electric free energy ($-\frac{1}{3}\varepsilon_0\varepsilon_a E^2 4\pi r^2 dr$, where r is the sphere radius). As the volume of the spherical shell $4\pi r^2 dr$ increases with increasing sphere radius, the most important is the spherical shell at the surface of the droplet—with radius $\approx R$. The electric free energy should be smallest if the largest spherical shell has concentric structure. Calculations, however, show that the lowest free energy is reached when the spherical shell with concentric structure is placed $\frac{1}{4}$ of the pitch inside ($r=R-\pi/2q$). This way the region close to the surface of the droplet is occupied with the structures similar to the concentric one and the energy is minimized.

2. Radial spherical structure

A droplet with RSS is not cylindrically symmetric so the electric free energy depends on both angles ϑ_0 and φ_0. The angle φ_0, however, enters only the amplitude function G in a very special way, that is, as a sum $\varphi_0+\Omega_0$ [Eq. (A2)]. Since Ω_0 is free to adjust appropriately to minimize the electric free energy, φ_0 dependence need not be treated separately. Similarly to the DSS, the angle ϑ_0 and function $G(\varphi_0+\Omega_0,Q)$ will take values such that the electric free energy is minimal. It follows from Eq. (A2) that there are again two different results that minimize the electric free energy according to the sign of G. For $G>0$ minimization gives $\vartheta_0=0$, while for $G<0$ it gives $\vartheta_0=\pi/2$. As for the DSS, the lowest minimum is reached for extreme values of G, $G=\pm 2/Q$. The first minimum corresponds to metastable (parallel) orientation and the

second one to stable (perpendicular) orientation of the $s=2\chi$ line [see Fig. 7(b)].

A description with successive spherical shells is consistent with the above calculations. For the RSS the structures in successive spherical shells are basically the same, but are mutually rotated (about the z axis) for the angle $\varphi=\Delta rq$ according to (1). The director lines on each spherical shell are circles with a common point on the $+z$ axis [10]. Since $\vec{E}$ is perpendicular to the χ line (i.e., to the z axis) we choose $\vec{E}$ to point along the $+x$ axis. When going from one spherical shell to the other there are two extreme possibilities: the largest director circle lies either in the xz plane or in the yz plane. In the first case, the electric free energy of the shell is maximal and in the other it is minimal [see Fig. 1(a)]. Similarly to the DSS, the electric free energy of the droplet with RSS is minimal when the spherical shell with the largest circle in the yz plane is placed $\frac{1}{4}$ of the pitch inside ($r=R-\pi/2q$).

[1] D. K. Yang and P. P. Crooker, Liq. Cryst. **9**, 245 (1991).
[2] H.-S. Kitzerow and P. P. Crooker, Liq. Cryst. **11**, 561 (1992).
[3] P. G. de Gennes, *The Physics of Liquid Crystals* (Clarendon, Oxford, 1993).
[4] R. J. Ondris-Crawford, M. Ambrožič, J. W. Doane, and S. Žumer, Phys Rev. E **50**, 4773 (1994).
[5] Y. Bouligand and F. Livolant, J. Phys. (Paris) **45**, 1899 (1984).
[6] H.-S. Kitzerow and P. P. Crooker, Liq. Cryst. **13**, 31 (1993).
[7] G. E. Volovik, Pis'ma Zh. Eksp. Teor. Fiz. **29**, 357 (1979) [JETP Lett. **29**, 322 (1979)].
[8] C. Robinson, J. C. Ward, and R. B. Beevers, Disc. Faraday Soc. **25**, 29 (1958).
[9] M. V. Kurik and O. D. Lavrentovich, Mol. Cryst. Liq. Cryst. **72**, 239 (1982).
[10] J. Bezić and S. Žumer, Liq. Cryst. **11**, 593 (1992).
[11] J. R. Quigley and W. J. Benton, Mol. Cryst. Liq. Cryst. **42**, 43 (1977).
[12] J. Bezić and S. Žumer (unpublished).
[13] N. D. Mermin, Physica (Utrecht) **B90**, 1 (1977).
[14] N. D. Mermin, Rev. Mod. Phys. **51**, 591 (1979).
[15] S. Žumer, S. Kralj, and J. Bezić, Mol. Cryst. Liq. Cryst. **212**, 163 (1992).
[16] J. Bezić and S. Žumer, Liq. Cryst. **14**, 1695 (1993).
[17] E. B. Priestly, P. J. Wojtowicz, and P. Sheng, *Introduction to Liquid Crystals* (Plenum, New York, 1975).
[18] A. Rapini and M. Papoular, J. Phys. (Paris) Colloq. **30**, C4-54 (1969).
[19] D. W. Allender, G. P. Crawford, and J. W. Doane, Phys. Rev. Lett. **67**, 1442 (1991).
[20] G. P. Crawford, D. W. Allender, and J. W. Doane, Phys. Rev. A **45**, 8693 (1992).
[21] P. Bucci and A. Golemme, J. Chem. Phys. **98**, 10070 (1993).